Preparation and Characterization of Nanocellular Poly(phenylquinoxaline) Foams. A New Approach to Nanoporous High-Performance Polymers

Samuel Merlet,[†] Catherine Marestin,*[,†] Fréderic Schiets,[†] Olivier Romeyer,[‡] and Régis Mercier[†]

Laboratoire des Matériaux Organiques à Propriétés Spécifiques (LMOPS), UMR 5041, CNRS-Université de Savoie, Chemin du Canal, BP 24, 69390 Vernaison, France, and Service de Microscopie, Université de Savoie, 73376 Le Bourget du Lac, France

Received September 29, 2006; Revised Manuscript Received January 19, 2007

ABSTRACT: This work deals with a new strategy for the elaboration of macro- to nanoporous materials. The adopted scheme involves the in-situ generation of foaming agents (CO_2 and isobutene) during the thermal treatment of a poly(phenylquinoxaline) (PPQ) film bearing thermolabile (*tert*-butyloxycarbonyl, i.e., Boc) groups (PPQ-Boc). For this purpose, a bis-diketone monomer having phenolic groups has been first synthesized and polymerized with a bis-diamine monomer. The resulting PPQ was postmodified by introducing Boc groups. After a kinetic and mechanistic study of the Boc thermal decomposition reaction, the influence of different experimental parameters on the final porosity formation has been investigated, such as the foaming temperature which is a key parameter. The porous materials obtained were characterized by different techniques (density, SEM, TEM) in order to determine the cell density as well as the size and morphology of the porous structure. Depending on the thermal treatment conditions, our strategy enables to obtain a wide range of porous materials, from nanoporous (10 nm, 10^{16} cells/cm^3) to macroporous (200−700 nm, 10^{12} cells/cm^3).

1. Introduction

In recent years there has been great interest in nanostructured materials to tailor novel molecular devices with specific properties. In this perspective, microporous (size < 2 nm) and mesoporous (2 < size < 50 nm)[1] (i.e., nanoporous) polymer materials can be considered as promising systems in many application fields such as nanofiltration,[2,3] sensoring,[4,5] and low-*k* dielectrics.[6−8] Therefore, the design of porous structure materials from the nano- to micrometer length scale represents a great challenge.

The most widely used approach to produce nanoporous materials is based on a template method.[9,10] Typically, an initial heterogeneous material is formed, containing a phase that can be removed from the whole material by either extraction or decomposition. This usually leads to a porous structure whose morphology corresponds to the removed template. Depending on the nature of the template, several cases can be distinguished. For example, polyimide−poly(propylene oxide) block copolymers were widely used as templates for the synthesis of nanoporous polyimide films.[11] Nanophase separation of the block copolymer and subsequent thermal decomposition of the poly(propylene oxide) block allow to obtain pore size of about 10 nm. However, the control of the phase-separated morphology of this block copolymer is not straightforward. A slightly different approach is based on the introduction of labile nanosized templates, such as dendritic, star-branched, or hyperbranched polymers, in a matrix (organic and/or inorganic). Hawker et al. made great advances in producing well-defined nanosized pore generators.[12,13] However, problems arise in the control of pore size due to porogen polydispersities, coalescence of pores, and the loss of structural integrity due to some pore collapse.[14]

An attractive alternative route for obtaining nanoporous polymers is to use a foaming process, a well-known technique to produce microcellular polymers.[15−22] This technique is based on a two-step process. First, the polymer is saturated under pressure with an inert gas, i.e., CO_2. This saturation step often needs long time equilibrium and high-pressure devices. The pressure is then quenched, and temperature is increased above the glass transition temperature of the plasticized polymer to generate porosity in the material. The resulting microstructure can be controlled by carefully choosing the processing conditions, i.e., saturation pressure, foaming temperature, and foaming time. Each of these parameters plays indeed an important role in the nucleation and growth mechanism which governs the final porosity morphology. However, the typical pore size thus obtained is rather large (1−10 μm). Recently, this approach has been applied to high-T_g polymers, i.e., polyimides and polysulfones, and resulted in a small open nanoporosity (20−50 nm).[23,24] In a recent study, Yokoyama et al. report the formation of closed nanopores within the nanodomains of CO_2-philic fluorinated blocks in polystyrene-based block copolymers monoliths.[25] This combination of a template-based method and a CO_2 foaming process leads to homogeneous nanopores with an average dimension of 20 nm.

In this paper we report the elaboration of a closed micro- to nanoporosity in high-performance polymer thin films, using a nonconventional foaming process.

Poly(phenylquinoxaline)s (PPQ) are good candidates for nanoporous materials because of their thermal stability, high T_g, good mechanical properties, and low dielectric constant.[26] Porous structures were obtained by the in-situ generation of foaming agents (CO_2 and isobutene) during the thermal treatment of PPQ-containing thermolabile groups (*tert*-butyloxycarbonyl, i.e., Boc). After describing the synthesis of the func-

* To whom correspondance should be addressed. E-mail: kmarestin@lmops.cnrs.fr.
[†] CNRS-Université de Savoie 5024.
[‡] Université de Savoie.

10.1021/ma062259t CCC: $37.00
Published on Web 02/21/2007

tionalized polymers and the foaming process key parameters, the characterization of the final porous materials will be presented. The influence of the experimental conditions on the final morphology will be discussed as well.

2. Experimental Section

2.1. Materials. Anisole, 1,4-phenylenediacetic acid, copper(II) bromide ($CuBr_2$), aluminum chloride ($AlCl_3$), di-*tert*-butyl dicarbonate (Boc_2O), 4-(dimethylamino)pyridine (DMAP) (Aldrich Chemical Co.), oxalyl chloride ($(COCl)_2$), and pyridine hydrochloride (Alfa Aesar Chemical Co.) were used as received. Dichloromethane (CH_2Cl_2) (Carlo Erba Chemical Co.), dimethyl sulfoxide (DMSO) (VWR Chemical Co.), *m*-cresol and *N*,*N*-dimetylformamide (DMF) (Merck Chemical Co.), and ethyl acetate (EtOAc) (SDS Chemical Co.) were used as received. *N*-Methylpyrrolidone (NMP) (SDS Chemical Co.) was dried at least for 24 h on 4 Å molecular sieves before use. 3,3′,4,4′-Tetraaminodiphenyl sulfone (Konishi Chemical Ind. Co.) was recrystallized in acetonitrile before use.

2.2. Characterization Methods. Thermomechanical analyses (TMA) were performed under nitrogen at a heating rate of 5 °C/min using a TA Instruments model Q400. Thermogravimetric analyses (TGA) were performed under helium at a heating rate of 10 °C/min (if not mentioned further) using a TA Instruments model 2950 thermogravimetric analyzer. Nuclear magnetic resonance (^{1}H NMR) spectra were recorded on a Bruker AC250 spectrometer operating at a resonance frequency of 250.13 MHz for ^{1}H and 62.89.MHz for ^{13}C. Tetramethylsilane was used as internal standard. For coupled TGA−time-resolved infrared analyses, TGA were performed under nitrogen at a heating rate of 10 °C/min using a TA Instruments model 2050 thermogravimetric analyzer; infrared spectra were obtained with a Nicolet Nexus FTIR. Inherent viscosities were determined with a Ubbelohde viscosimeter. Flow times were measured from 0.50 g/dL NMP solution at 30.0 ± 0.1 °C.

2.3. Synthesis of Reagents and Monomers. *1,4-Bis(4-methoxyphenacyl)benzene (**1**).* To a suspension of *p*-phenylenediacetic acid (3.00 g, 15.5 mmol) in 50 mL of CH_2Cl_2 were added oxalyl chloride (7.80 g, 61.4 mmol) and 4 drops of DMF before heating the solution at 40 °C for 3 h. The solution was then cooled to room temperature. The solvent and oxalyl chloride excess were removed by evaporation under reduced pressure. The resulting diacid chloride was dissolved in CH_2Cl_2 and added dropwise to a −5 °C solution containing anisole (8.00 g, 74.0 mmol), anhydrous $AlCl_3$ (6.00 g, 45.1 mmol), and 100 mL of CH_2Cl_2. During the addition the reaction temperature was kept below 0 °C. After complete addition, the dark red reaction mixture was stirred at 0 °C for 1 h and poured into ice and hydrochloric acid. Evaporation of the solvent and excess of anisole under reduced pressure led to a white solid in suspension in the acidic solution. The solid was filtered, washed with water until neutrality, and dried overnight at 100 °C under reduced pressure to yield 1 (5.74 g, 99%).^{1}H NMR (d_6-DMSO, 294 K): δ (ppm) 8.02 (d, 4H, J = 8.9 Hz), 7.19 (s, 4H), 7.04 (d, 4H, J = 8.9 Hz), 4.27 (s, 4H), 3.83 (s, 6H). ^{13}C NMR (d_6-DMSO, 360 K): δ (ppm) 192.4, 163.2, 133.3, 130.4, 129.6, 129.1, 113.7, 55.1, 44.1.

*1,4-Bis[(4-methoxyphenyl)glyoxalyl]benzene (**2**).* In a mixture of 40 mL of DMSO and 40 mL of EtOAc were added 1,4-bis(4-methoxyphenacyl)benzene (5.80 g, 15.5 mmol) and $CuBr_2$ (13.80 g, 61.8 mmol). The solution was heated under reflux for 48 h. The solution was cooled and poured into water. The yellowish solid was filtered and extracted by Soxhlet in CH_2Cl_2 for 3 days to remove insoluble copper(I) salts. Drying at 80 °C under reduced pressure yields **2** as a yellow solid (4.70 g, 75%). ^{1}H NMR (d_6-DMSO, 360 K): δ (ppm) 8.08 (s, 4H), 7.90 (d, 4H, J = 8. Hz), 7.12 (d, 4H, J = 8.9 Hz), 3.88 (s, 6H). ^{13}C NMR ($CDCl_3$/CF_3-COOD 1:1, 294 K): δ (ppm) 196.7, 195.9, 168.2, 138.6, 134.9, 132.0, 126.0, 116.4, 56.7.

*1,4-Bis[(4-hydroxyphenylglyoxalyl]benzene (**3**).* 1,4-Bis[(4-methoxyphenyl)glyoxalyl]benzene (4.50 g, 11.2 mmol) and pyridinium hydrochloride (13.00 g, 112 mmol) were heated together at 200 °C for 15 h under a slight nitrogen flow. The mixture was cooled, and compound **3** was precipitated by adding 1.0 M aqueous hydrochloric acid into the reaction flask. The resulting brown solid was filtered, washed with water until pH neutrality, and dissolved in aqueous potassium carbonate solution (5 g in 200 mL of H_2O). Filtration of the resulting solution provided a clear yellow solution which was neutralized with hydrochloric acid to give a yellow solid. The solid was filtered and dried overnight at 100 °C under reduced pressure to yield **3** (4.13 g, 90%). ^{1}H NMR (d_6-DMSO, 294 K): δ (ppm) 10.99 (s, 2H), 8.09 (s, 4H), 7.82 (d, 4H, J = 8.9 Hz), 695 (d, 4H, J = 8.9 Hz). ^{13}C NMR (d_6-DMSO, 294 K): δ (ppm) 192.4, 192.0, 164.5, 136.8, 132.7, 130.2, 123.5, 116.3.

2.3. Polymerization of Poly(phenylquinoxaline) (PPQ-OH). To a three-necked round-bottom flask equipped with a nitrogen inlet and a mechanical stirrer were added 1,4-bis[(4-hydroxyphenyl)-glyoxalyl]benzene (2.6660 g, 7.12 mmol), 3,3′,4,4′-tetraaminodiphenyl sulfone (1.9811 g, 7.12 mmol), and 19 mL of *m*-cresol (80 wt %). The mixture was stirred at 60 °C for 24 h. The brown viscous solution was diluted with *m*-cresol and cooled to room temperature. The polymer was precipitated in methanol. The yellow, fibrous PPQ-OH was ground into pieces and collected by filtration, washed with methanol, and stirred overnight in methanol. The polymer was dried overnight at 100 °C under reduced pressure. ^{1}H NMR (d_6-DMSO, 360 K): δ (ppm) 9.57 (s, 2H), 8.79 (s, 2H), 8.30 (s, 4H), 7.54 (s, 4H), 7.37 (d, 4H, J = 7.5 Hz), 6.77 (d, 4H, J = 7.5 Hz).

2.4. Postmodification of PPQ-OH (PPQ-Boc). PPQ-OH (2.00 g, 6.88 mmol OH) was dissolved in 20 mL of dried NMP. To this solution was added Boc_2O (1.72 g, 7.88 mmol). The reacting mixture was stirred at ambient temperature under a nitrogen flow, and a solution of DMAP (0.058 g, 0.47 mmol) in dried NMP (2 mL) was added dropwise for 5 min. The solution was stirred an additional 12 h. The polymer was then precipitated in methanol. The yellow, fibrous PPQ-Boc was ground into pieces and collected by filtration, washed with methanol, and stirred overnight in methanol. The polymer was dried overnight at 50 °C under reduced pressure. ^{1}H NMR ($CDCl_3$, 294 K): δ (ppm) 8.96 (d, 2H, J = 17.2 Hz), 8.27 (d, 4H, J = 7.7 Hz), 7.56 (m, 8H), 7.16 (m, 4H), 1.52 (s, 18H).

2.5. Film Preparation. Both PPQ-OH and PPQ-Boc thin films were prepared by casting a 15 wt % polymer solution in NMP on a glass plate. The casted films were dried under nitrogen at 50 °C for 24 h. Subsequently, the homogeneous dense films were removed from the glass support and immersed in a methanol bath at room temperature for 48 h in order to remove the traces of NMP. The washed films were then dried at 50 °C under vacuum for 24 h and analyzed by TGA. The remaining solvent content was measured to be systematically lower than 0.1 wt %. Depending on the viscosity of the polymer solution, the dense films thickness ranges from 20 to 50 μm.

2.6. Porous Films Formation and Characterization. PPQ-Boc dense films (1 cm × 1 cm) were placed in a convectional oven (Heraeus UT6060), under a nitrogen atmosphere and at different controlled temperatures (foaming temperature, T_f). After 60 s (foaming time), the films were removed from the oven and cooled to ambient temperature.

The mass density of porous film was measured by a flotation method. The sample was immersed in a mixture of two miscible solvents having different densities. Their proportion was adjusted until isodensity was obtained. The determined mixture density corresponded to the sample density. Depending on the density of the sample, different solvent mixtures were used (sodium bromide aqueous solutions, cyclohexane/tetrachloroethene mixtures, cyclohexane/petroleum ether mixtures). No liquid uptake in the foamed sample (which would have overestimated the sample density) could be observed during the measurements. The obtained mass densities are average values of the entire polymer sample, i.e., the foamed core part including the integral dense skin.

The porous morphology of the foamed polymer films was investigated by scanning electron microscopy (SEM) and transmission electron microscopy (TEM). SEM was performed on a Leica

Scheme 1. Synthetic Route to 1,4-Bis[(4-hydroxyphenyl)glyoxalyl]benzene

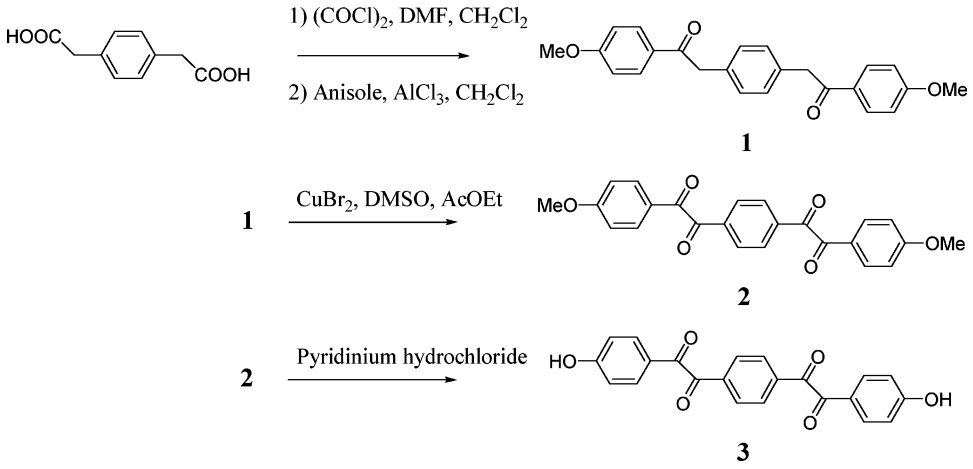

Scheme 2. Synthesis and Boc Functionalization of PPQ-OH

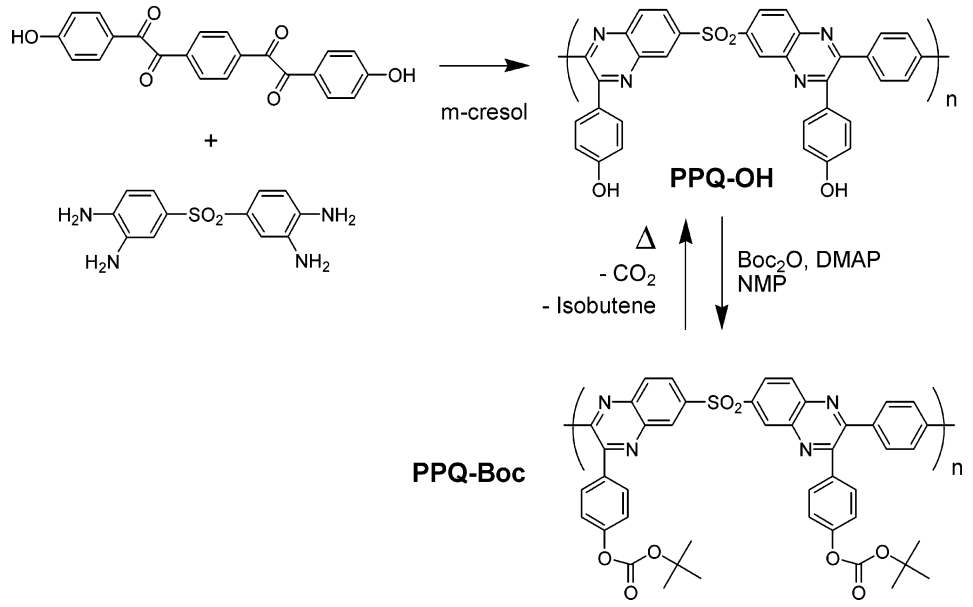

Stereoscan 440 scanning microscope. The samples were freeze fractured in liquid nitrogen and sputter-coated with carbon (0.1 mbar and 30 mA for 2 min). TEM was performed on Philips CM120 microscope operating at 80 kV. The polymer samples were embedded in an epoxy resin and microtomed in cross section. The resulting sections were 70−80 nm thick. The resulting micrographs were analyzed by ImageJ software. Usually, micrographs containing 150−200 cells were used in the image analysis. The cell density N_0 is the number of cells nucleated per unit volume (cm^3) of the original unfoamed polymer. It was calculated from the micrographs using the method suggested by Kumar and Weller:[18]

$$N_0 = [nM^2/A]^{3/2}[1/(1 - V_f)] \quad (1)$$

where V_f is the void fraction, n the number of cells in the micrographs, M the magnification of the micrograph, and A the area of the micrograph (cm^2).

3. Results and Discussion

3.1. Preparation of Boc-Grafted PPQ and Structural Characterizations of Decomposition. The *tert*-butyloxycarbonyl (Boc) groups are usually used in the photoresist technology.[27,28] They can be cleaved either in acidic conditions[28,29] or under a thermal treatment.[30,31] In both cases, the parent backbone is regenerated by the release of CO_2 and isobutene. The Boc group acts as a protecting agent for a wide range of functions, such as amine,[32,33] alcohol, phenol, and amide.[34] In this work, we chose to introduce Boc from PPQ side-chain phenol groups.

A bis-diketone having phenol groups, 1,4-bis[(4-hydroxyphenyl)glyoxalyl]benzene (**3**), was prepared according to a previously reported pathway,[35] but with slight modifications of known procedures[36] (Scheme 1).

The bis-diketone (**3**) was obtained as a polymer grade monomer and polycondensed with 3,3′,4,4′-tetraaminodiphenyl sulfone under classical poly(phenylquinoxaline)s polymerization conditions.[26] The resulting polymer presents reactive side-chain phenol groups which could be then transformed in thermolabile Boc groups (Scheme 2).

The postmodification of the phenol groups to PPQ-Boc was carried out by a conventional procedure using di-*tert*-butyldicarbonate (Boc_2O) and DMAP,[37] in NMP at ambient temperature. Quantitative Boc grafting was evidenced by ^1H NMR (Figure 1a,b) and by thermogravimetry (Figure 2). As shown by the thermogram in Figure 2, the thermolabile Boc groups start decomposing at temperature around 130 °C with a maximum decomposition speed at 180 °C. The experimental weight loss (24.4 wt %) is in good accordance with a theoretical total decomposition (25.6 wt %). Moreover, the readily recovering of the PPQ-OH structure is controlled by ^1H NMR, as shown in Figure 1c.

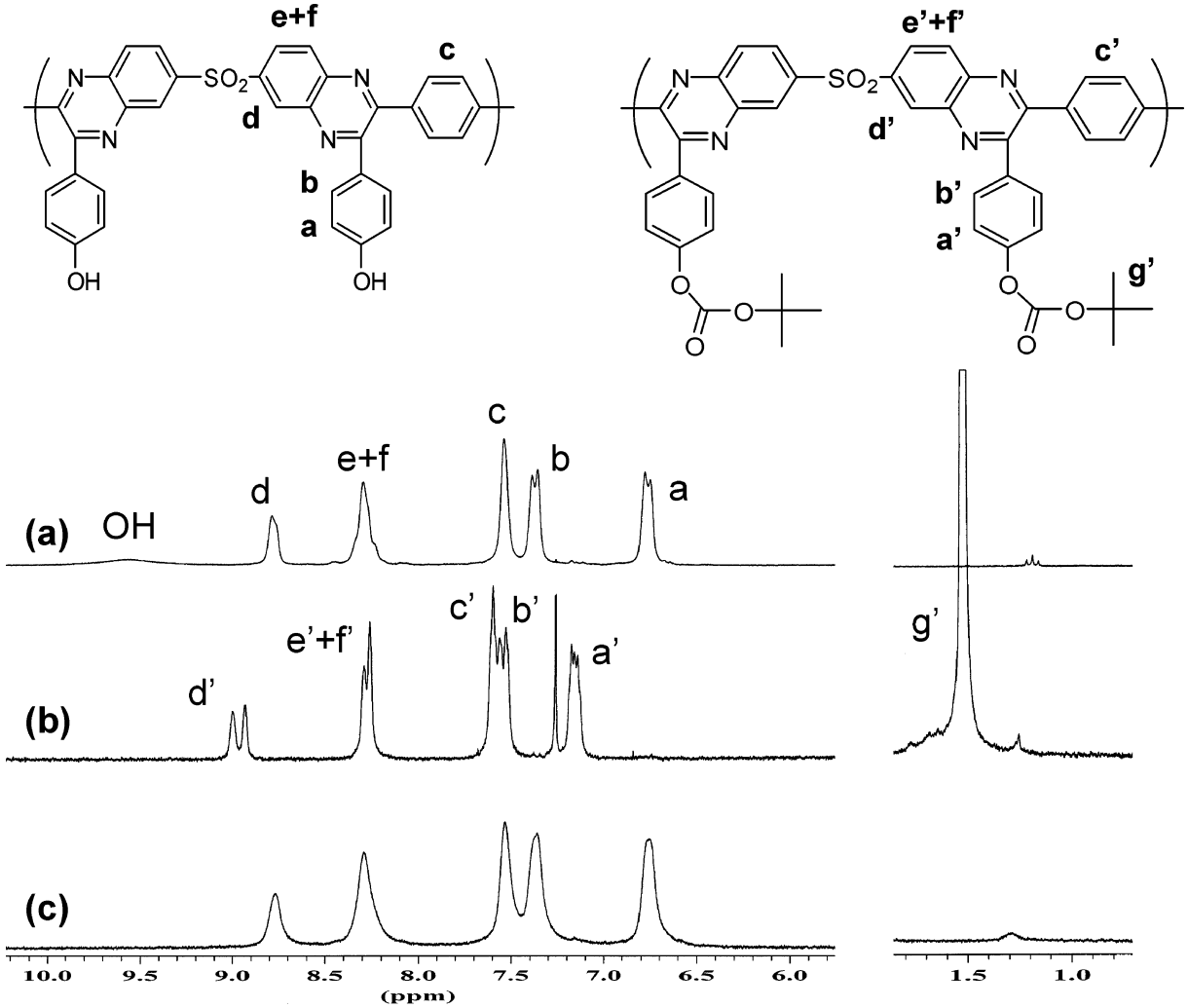

Figure 1. [1]H NMR spectra of PPQ-OH (a), PPQ-Boc (b), and the decomposed PPQ-Boc (c) treated at 200 °C for 15 min under an inert atmosphere.

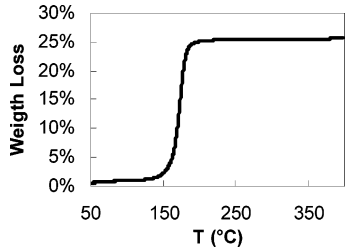

Figure 2. TGA analysis of PPQ-Boc with a heating rate at 10 °C/min and under nitrogen.

Table 1. Properties of Synthesized PPQ-OH, PPQ-Boc, and the Decomposed PPQ-Boc

	solubility				
polymer	CH_2Cl_2	DMSO	NMP	T_g (°C)[c]	η_{inh} (dL/g)
PPQ-OH	×	√	√	370	0.50
PPQ-Boc	√	×	√	>275[b]	0.42
PPQ-Boc[a]	×	×	√	370	0.86

[a] PPQ-Boc treated at 200 °C for 15 min under an inert atmosphere. [b] Determined from a model polymer PPQ-dimethylbutyrate. [c] Determined from TMA analysis.

It is worth mentioning that, instead of a postmodification of PPQ-OH, the direct introduction of Boc group through the polycondensation reaction of a Boc-containing bis-diketone was not possible. Indeed, the polymerization conditions (*m*-cresol, 60 °C, 24 h) were found to result in the decomposition of Boc groups.

Self-standing films could be obtained from all prepared polymers and present a very good thermal stability ($T_{5\ wt\ \%\ loss}$ > 450 °C). It is well-known that the mere modification of the polymer backbone structure could have a great influence on its final properties. As reported elsewhere on different polymers,[38] the presence of Boc groups significantly changes the solubility of the poly(phenylquinoxaline)s, especially in chlorinated organic solvents such as CH_2Cl_2 (Table 1).

The presence of phenol groups drastically changes the T_g of the polymers. Indeed, a 50 °C difference in T_g could be measured between a PPQ-OH (T_g = 370 °C) and the analogous PPQ without OH groups (T_g = 320 °C).[39] This could be attributed to the acid−base interaction between OH groups and the quinoxaline rings (slight basic character). During the thermal treatment devoted to the elaboration of porous materials, the polymer backbone structure changes from PPQ-Boc to PPQ-OH. As a consequence, T_g of the film is expected to evolve as well. Unfortunately, an exact value of the T_g of PPQ-Boc was impossible to measure as Boc groups start to decompose at 130 °C. A PPQ-Boc model based on the ester of PPQ-OH with dimethylbutyric acid (PPQ-dimethylbutyrate) was then synthesized to mimic the PPQ-Boc behavior. Once again, any accurate measurement of T_g could be made as this polymer start degrading before (for T < 275 °C).

Whereas their chemical structures are similar as shown by [1]H NMR (Figure 1a,c), the PPQ-OH resulting from a PPQ-Boc decomposition has a higher inherent viscosity than the initial

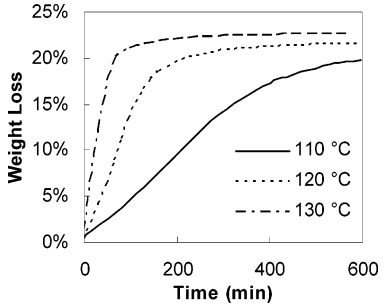

Figure 3. Isothermal decompositions of PPQ-Boc under nitrogen at different temperatures.

polymer. As free ortho-diamine end groups could be present on PPQ-OH chains, a possible explanation for this observation is that the polymer molecular weights increase during the postmodification step, as previously proposed by Gain et al.[40] Indeed, these authors report similar results by studying a polyimide-Boc and its thermally treated analogue. They explained the inherent viscosity increase by a chain coupling mechanism through the formation of urea linkages between amino polyimide end goups during the postmodification with Boc_2O. In order to validate this hypothesis, PPQ-OH amino end groups were blocked by the addition of 5 mol % of benzil at the end of the polymerization. The polymer thus obtained, end-capped with nonreactive groups (PPQ-OH′), was postmodifed (PPQ-Boc′) and thermally treated. The inherent viscosity of these polymers was $\eta_{PPQ-OH'} = 0.52$ dL/g, $\eta_{PPQ-Boc'} = 0.39$ dL/g, and $\eta_{PPQ-Boc'\,dec} = 0.59$ dL/g. Although a slight increase of the inherent viscosity was observed after the Boc decomposition, the difference between the two viscosity values is not really significant to be attributable to chain growth.

3.2. Kinetic Characterizations of Decomposition. The Boc decomposition temperature which affects the reaction kinetic and the relative evolution of both CO_2 and isobutene is the key parameter for the foaming process. Therefore, the decomposition was studied by TGA under isothermal conditions. Several isotherms thermogram are plotted in Figure 3 and suggest the existence of a catalytic decomposition mechanism.

The calculated activation energy (determined according to the Ozawa−Flynn−Wall method)[41] varies between 128 and 132 kJ/mol, depending on the degree of decomposition. These values seem to give additional credit to a catalytic mechanism, whose activation energy is typically around 120 kJ/mol,[29,42] rather than a noncatalytic one, which is usually associated with a higher activation energy of 190 kJ/mol.[31] One possible explanation for that result could be related to the formation of phenol groups in the course of the Boc deprotection. Indeed, as reported elsewhere,[43,44] carbonate group decomposition is well-known to be catalyzed by acidic media, and in this regard the deprotected phenols are expected to have a sufficient acidic character to play a catalytic role. Another probable source of acidic protons is residual *m*-cresol present in the polymer. Moreover, at the very early stage of the decomposition process, no higher activation energy could be observed. This could be explained by the presence of either nonfunctionalized phenolic or *m*-cresol traces, which could not however be detected by proton NMR.

A TGA coupled time-resolved IRTF analysis gave a complementary description of the decomposition Boc reaction. More than a simple characterization of the released gases (Figure 4a), their relative evolution was determined by following their absorbance at 2363 and 887 cm^{-1} and normalized with the respective integrated area (Figure 4b). As a result, both gases

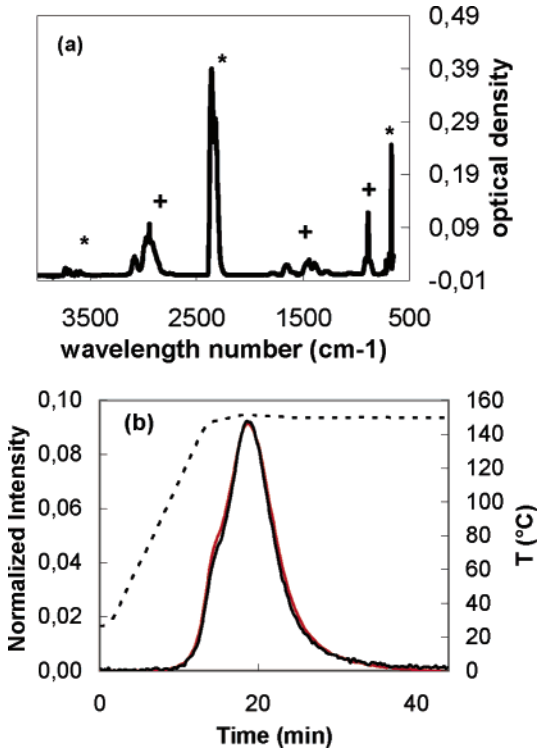

Figure 4. (a) IR spectrum of the generated gases, CO_2 (∗) and isobutene (+). (b) Relative evolution of CO_2 (red line) and isobutene (black line) during a temperature ramp followed by a 150 °C isotherm (dotted line).

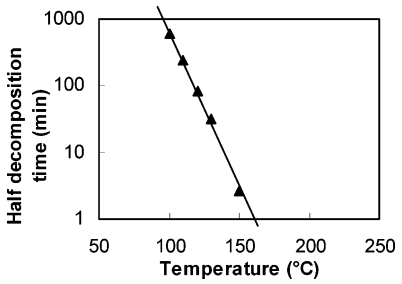

Figure 5. Half-time decomposition of PPQ-Boc as a function of the temperature.

were shown to be simultaneously produced. Unfortunately, this observation cannot either infirm or confirm any commonly accepted Boc deprotection mechanism (catalytic[28,29] and noncatalytic[31]).

Isothermal TGA were performed in order to determine the decomposition rate vs the temperature. As represented in Figure 5, half decomposition time varies exponentially with the temperature. From these results, a limit temperature could be extrapoled (ca. 160 °C), above which the complete decomposition reaction occurs with time inferior or equal to 2 min. In order to have a complete and rapid decomposition reaction, the temperature chosen in this study for obtaining porous materials was systematically higher than this limit temperature.

3.3. Preparation and Characterization of Porous Films. Heat and mass transport phenomena are expected to affect the foaming process. As a consequence, the important parameters in our process are the following: film thickness, foaming temperature (T_f), and foaming time. The influence of these parameters on the foam morphology was there systematically studied to get a thorough understanding of the foaming process and were optimized to obtain homogeneous cell size distribution, maximum cell density, and minimum mass density.

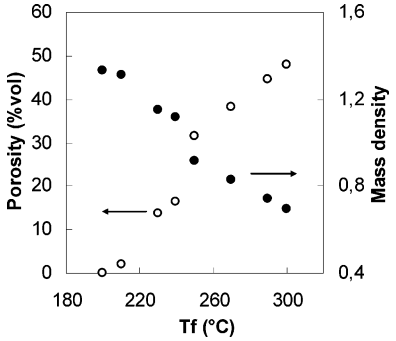

Figure 6. Porosity of the foams as a function of the thermal treatment (50 μm thick films).

3.3.1. Influence of Foaming Time. Various samples (20−40 μm thick films) were thermally treated at T_f (200−300 °C) for different foaming times (60 s to 15 min). The resulting films were characterized by ^{1}H NMR and density measurements. In all cases ^{1}H NMR confirmed a total decomposition of the Boc groups. In addition, the sample density decreases as a function of the foaming temperature, suggesting an increasing porosity fraction with temperature. Considering a given foaming temperature, no significant variation of density could be observed over the range of foaming times (60 s to 15 min). We then believe that the foaming process is extremely rapid, and a thermal treatment as short as 60 s should be sufficient for the elaboration of porous materials. An other important result is the good stability of the porous structure formed over time for such high temperatures.

3.3.2. Influence of Foaming Temperature. In a conventional foaming process, it is well-established that the porosity formed from a nucleation−growth mechanism occurs at temperatures above the polymer/gas mixture T_g. As a consequence, in this study, the porosity formation which is expected to be produced also by a nucleation−growth mechanism will highly depend on both the foaming temperature and the PPQ/gas mixture T_g. Polymers are known to be plasticized by the presence of gases, particularly CO_2,[45] and some theoretical models are developed to predict the polymer/gas mixture T_g.[46] Although a lot of results are reported in the literature about CO_2-plasticized polystyrenes or polycarbonates, to our knowledge, no data concerning PPQ plastificization are available. In addition, the nonequilibrium state, due to diffusion out of the film, remains problematic for the accurate determination of T_g by a conventional method. Different PPQ-Boc samples were foamed for 60 s at temperatures ranging from 200 to 300 °C. The mass density of the resulting films as well as the porosity estimated from these measurements is reported in Figure 6.

Despite a complete decomposition of the thermolabile groups (as witnessed by ^{1}H NMR), no porous structure could be evidenced by a density measurement when the film was treated below 210 °C (Figure 6). This foaming temperature was then assumed to be under the polymer/gas mixture T_g, and the absence of porosity was explained by the fact that the glassy state of the system prevents any viscoelastic deformations. As a 10% film thickness decrease could be measured, we believe that the voids created by the Boc decomposition do not reach the thermodynamically viable critical size and collapsed through local relaxations.

For higher foaming temperatures (T_f > 210 °C) the observed density decrease suggests the formation of porosity. As a consequence, the polymer/gas mixture T_g could be estimated around 200−210 °C. Above this temperature, the system viscosity is sufficiently low to enable chain mobility and thus the foam formation under the blowing effect of the produced gases. In addition, as described in a conventional CO_2 foaming process, porosity increases with foaming temperature due to a lower polymer/gas mixture viscosity which leads to higher cell growth.

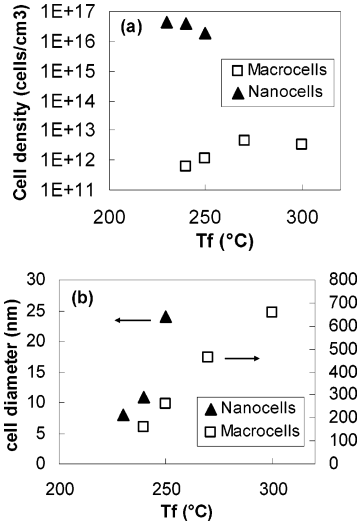

Figure 7. (a) Size evolution of nanocells (<50 nm) and macrocells (>50 nm) with the foaming temperature (T_f). (b) Dependences of the density of nanocells and macrocells with the foaming temperature.

It is moreover interesting to note that no collapse of the porous structure was observed in this temperature range (200−300 °C). This is essentially due to the high T_g of the final system ($T_{g,PPQ-OH}$ = 370 °C).

The cross section of the samples foamed at different temperatures ranging from 210 to 300 °C was observed by SEM and TEM in order to characterize the morphology. As shown in Figure 7, different porous morphologies could be distinguished. For T_f < 240 °C, a homogeneous nanoporous structure was formed (size < 50 nm). For 240 ≤ T_f < 250 °C a bimodal size distribution was observed because of the formation of macropores (size > 50 nm). For T_f > 250 °C nanocells were no more present, but homogeneous ultramicrocellular foam was observed. We will then refer to nanocells for pores having size < 50 nm and macrocells for pores having size > 50 nm.

For low foaming temperature (T_f < 240 °C) a homogeneous closed nanoporous structure (average size of 8 nm) was observed by TEM (Figure 8b) as well as a high nanocell density (10^{16} cells/cm^3). Nanofoams with such a high cell density and small pores have not yet been reported in the literature from a conventional foaming process. According to the classical nucleation theory, such a high cell density could be explained by a high nucleation density, which results from a high gas concentration into the polymer. This gas concentration is believed to be a key factor to influence both the cell size and the density during the foaming process. It should be noted that 2−10 wt % CO_2 can typically be dissolved in high-T_g polymers at 25 °C under 50 bar.[23,47,48] Handa et al. have examined the saturation of PMMA under lower temperature conditions (−0.2 °C) in order to increase the CO_2 content up to 22.5 wt %. The resulting ultramicrocellular foam showed a 350 nm closed cell size with a density of 4.4 × 10^{13} cells/cm^3. Krause et al. have however demonstrated that CO_2 concentration above 50 cm^3/cm^3 of polymer (ca. 7 wt %) could lead to high-T_g poly(imide)s nanofoams with smaller size (20−100 nm, 10^{14} cells/cm^3), but with an open cellular structure. In the present work, the calculated amount of released gases is respectively 12.6 and 15.5 wt % of CO_2 and isobutene. It is then important to note

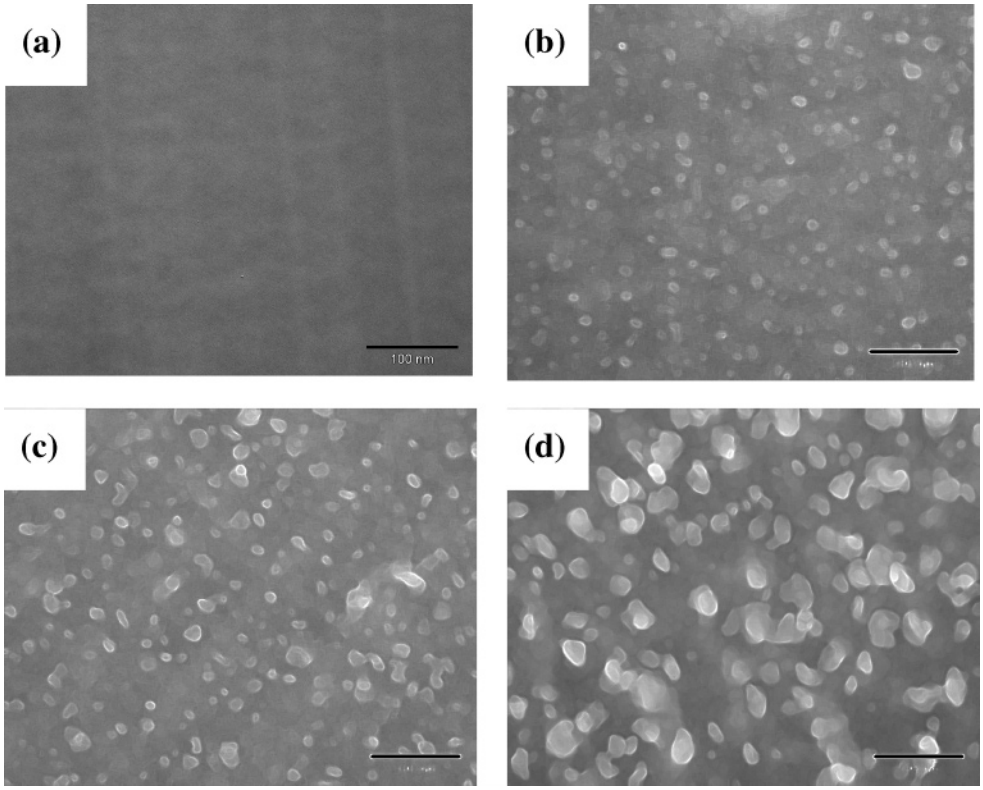

Figure 8. TEM images of nanofoamed PPQ at 210 (a), 230 (b), 240 (c), and 250 °C (d). The bars indicate 100 nm.

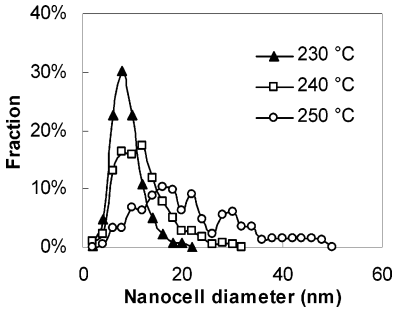

Figure 9. Nanocell size distribution in a foamed PPQ film at different foaming temperatures: 230, 240, and 250 °C for 60 s.

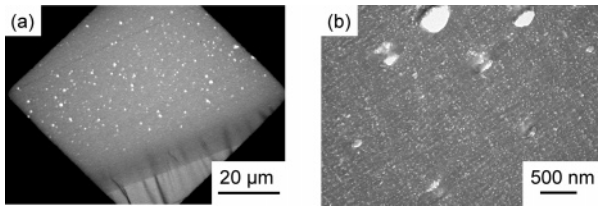

Figure 10. TEM images of nanofoamed PPQ at 250 °C at two different magnifications.

that this approach enables a higher gas generation in the polymer than the conventional gas saturation method. In addition, no bicontinuous structure could be observed in TEM/SEM images. It is obvious that the properties of the polymer, and particularly its T_g, play an important role in the porosity formation and on the final porous morphology. We believe that the nanoporous structure could result from an homogeneous nucleation mechanism that would lead to thermodynamically stable nanonuclei. The very small size of observed nanocells could be related to a very high viscosity of the system at low foaming temperature which prevents an extensive cell growth.

With increasing foaming temperature (at 230, 240, and 250 °C) the average nanocell size varies from 8 to 11 and 24 nm, respectively (Figure 7a). In addition, the cell size distribution broadens as shown in Figure 9. One can consider that the increasing cell size with the foaming temperature is consistent with a classical nucleation and growth mechanism. However, the cell density should increase as well, which is not observed (Figure 7b). The decrease in nanocell density with temperature as well as the evolution of the cell shape, from spherical to slightly distorded, would suggest a partial cell coalescence.

In addition, at a macroscopic scale, a macroporosity (160−260 nm) can as well be observed. The foaming temperature range 240−250 °C is thus characterized by a coexistence of nano- and macrocells, as shown in TEM images (Figure 10). Bimodal distributions have already been reported in the literature and could have various origins, such as additional time-delayed nucleation in an homogeneous system[22] or heterogeneous nucleation.[25,49] However, such considerations are not valuable in the present study. Since we believe that nanocells result from an homogeneous nanonucleation, a possible explanation for this bimodal distribution is the preferential growth of macrocells. Macrocells are known to be thermodynamically more stable than nanocells, since the latter have a larger surface area. Considering that some nanocells could lead to larger pores by coalescence, the system total energy can be decreased by a preferential growth of bigger cells, thus reducing the total interfacial area. In this perspective, this interfacial area reduction process, the so-called Ostwald ripening phenomenon,[50] could explain the depletion of nanocells and even their total disappearance for higher foaming temperature.

When PPQ-Boc films are treated above 250 °C, ultramicrocellular foams (average closed size of 660 nm and 4×10^{12} cells/cm^3) were formed, as presented in SEM images (Figure 11). The porous structure morphology is similar to those obtained with a conventional foaming process, with a closed cells containing porous core and a dense skin. However, the cell density of the ultramicrocellular PPQ was significantly higher (1−2 orders of magnitude) than that reported for the most

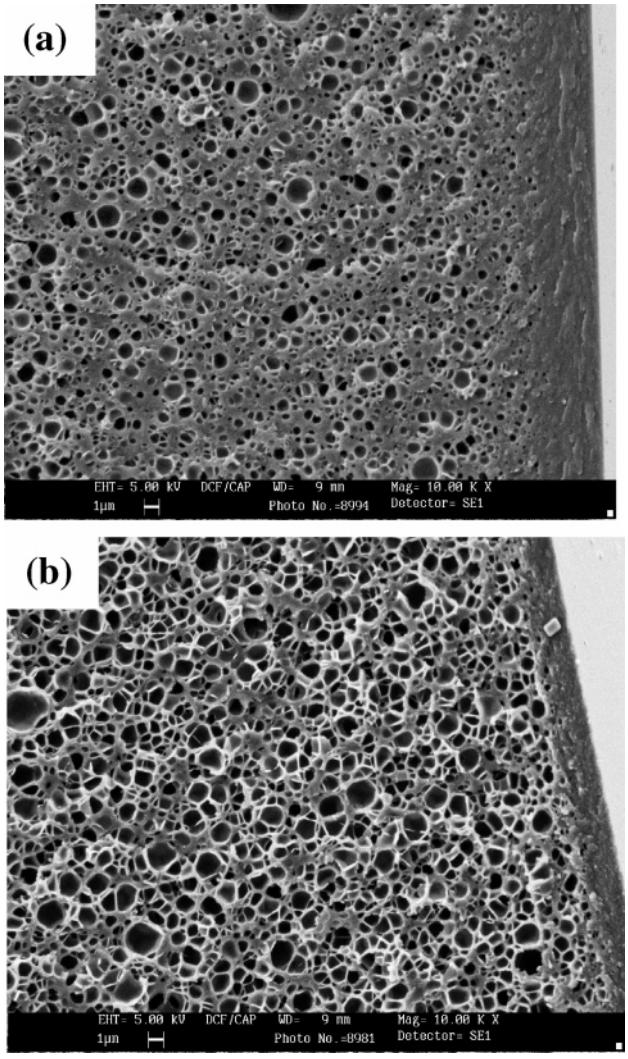

Figure 11. SEM micrographs of PPQ foamed at 270 (a) and 300 °C (b). Thickness of films are about 50 μm. Magnification: 20 000; the white horizontal bar indicates 1 μm.

studied high-T_g polymer foams (polysulfones, poly(ether sulfone)s, poly(ether imide)s).[47,48] A considerable smaller size could be evidenced in this case as well, which could be attributed to the both high nucleation density and the relatively low cell growth (due to the high-T_g PPQ).

3.3.3. Influence of Film Thickness. Considering the heat transfer and gas diffusion phenomena, the sample thickness has to be taken into account. As reported by Krause et al.,[48] heat transfert time scale (about 15 s) is comparable with foaming time when millimeter thick films are considered, whereas it becomes negligible (0.05 s) for micrometer thick films. As the thickness of the films studies in this work ranged from 2 to 50 μm, heat transfer phenomena were neglected. Gas diffusion, however, is responsible for the typical foamed-core/dense-skin morphology, as observed in Figure 11. When the gas is released in the film, it can diffuse either in the nucleated cells, resulting thus in their growth, or out of the film through the film surface. It is then a question of length scale, leading to the dense polymer near its surface.

Although for a given foaming temperature the skin thickness was found to be independent of the initial thickness, it is clearly shown in Figure 12 that the skin became thinner with higher foaming temperatures. A possible explanation for this result is that the surface requires a higher temperature to be foamed, resulting from a higher local T_g near the surface, due in turn to

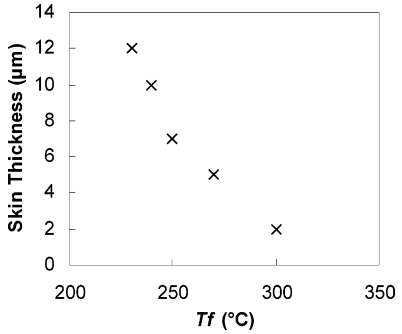

Figure 12. Evolution of the skin thickness with the foaming temperature.

a lower gas concentration. It is indeed commonly assumed in conventional process that the gas concentration inside the film has a Gaussian profile with a lower surface value. Depending on the diffusion time (transfer time between high-pressure vessel and the foaming bath), this profile has a more or less pronounced amplitude.[51]

Whereas the films with an initial thickness ranging from 20 to 50 μm and treated at 300 °C for 60 s present a porosity in the same order of magnitude (from 44 to 48 vol %), no porous structure could be observed on the very thin films (2 μm) thermally treated in identical conditions. This is believed to be the consequence of the skin thickness whatever the initial film thickness. A critical film thickness would then exist for the foaming process to be successful. This critical thickness should correspond to 2 × skin thickness for a given T_f. Such a critical thickness has already been reported by Doshi et al.[52] The authors demonstrate by mathematical modeling the existence of a thickness limit under which diffusion out of the film prevails on the cell growth mechanism, and thus no foam structure could be obtained. This thickness limit depends on the diffusion parameters of the gas/polymer system and on the processing parameters.

4. Summary

Boc-containing PPQs were successfully prepared by post-modification of PPQs bearing hydroxyphenyl groups which were obtained by polycondensation of hydroxyphenyl containing bis-diketone with a bis-diamine. The Boc decomposition reaction which generates both CO_2 and isobutene was well characterized in terms of temperatures and kinetics. Adapted thermal treatment leads to the formation of porous PPQs through a very probable nucleation and growth mechanism. The foamed PPQs showed relatively small cell size and high cell density which was attributed respectively to a high nucleation (high gas generation into the polymer) and a moderated growth of the cells (high T_g of the polymer). Our results show that the foaming temperature is a key parameter. A careful choice of T_f can lead to a fine-tune of the porosity from nanoscale (<50 nm) to macroscale (>50 nm) size. For 210 < T_f < 230 °C homogeneous nanoporous (8 nm, 4.4×10^{16} cells/cm^3) PPQ could be obtained with a narrow distribution and a significant volume fraction (14 vol %). With increasing T_f to 250 °C, a coexistence of nano- and macrocells was evidenced. At higher T_f (>250 °C) ultramicrocellular foams were obtained (660 nm, 4×10^{12} cells/cm^3).

Acknowledgment. The French ministry is gratefully acknowledged for its financial support (ACI Jeune Chercheur No. 4020).

References and Notes

(1) *IUPAC Compendium of Chemical Terminology*, 2nd ed.; IUPAC, 1997.

(2) Liu, J.; Teo, W. K.; Chew, C. H.; Gan, L. M. *J. Appl. Polym. Sci.* **2000**, *77*, 2785−2794.
(3) Chew, C. H.; Li, T. D.; Gan, L. H.; Quek, C. H.; Gan, L. M. *Langmuir* **1998**, *14*, 6068−6076.
(4) Mintova, S.; Rein, T. *Microporous Mesoporous Mater.* **2001**, *50*, 159−166.
(5) Shi, H. Q.; Tsai, W.; Garrison, M. D.; Ferrari, S.; Patner, B. D. *Nature (London)* **1999**, *398*, 593−597.
(6) Yang, S.; Mirau, P. A.; Pai, C.; Nalamasu, O.; Reichmanis, E.; Pai, J. C.; Obeng, Y. S.; Seputro, J.; Lin, E. K.; Lee, H.; Sun, J.; Gidley, D. W. *Chem. Mater.* **2002**, *14*, 369−374.
(7) Hawker, C. J.; Hedrick, J. L.; Miller, R. D.; Volksen, W. *MRS Bull.* **2000**, *25*, 54−58.
(8) Yang, C. M.; Choi, A. T.; Par, F. M.; Tsai, T. G.; Chao, K. J. *Adv. Mater.* **2001**, *13*, 1099−1102.
(9) Hentze, H. P.; Antonietti, M. *Curr. Opin. Solid State Mater. Sci.* **2001**, *5*, 343−353.
(10) Liu, T.; Burger, C.; Chu, B. *Prog. Polym. Sci.* **2003**, *28*, 5−26.
(11) Hedrick, J. L.; Carter, K. R.; Labadie, J. W.; Miller, R. D.; Volksen, W.; Hawker, C. J.; Yoon, D. Y.; Russell, T. P.; McGrath, J. E.; Briber, R. M. *Adv. Polym. Sci.* **1999**, *141*, 1−43.
(12) Hedrick, J. L.; Magbitang, T.; Connor, E. F.; Glauser, T.; Volksen, W.; Hawker, C. J.; Lee, V. Y.; Miller, R. D. *Chem.—Eur. J.* **2002**, *8*, 3309−3319.
(13) Heise, A.; Nguyen, C.; Malek, R.; Hedrick, J. L.; Frank, C. W.; Miller, R. D. *Macromolecules* **2000**, *33*, 2346−2354.
(14) Treichel, H. *J. Electron. Mater.* **2001**, *30*, 290−298.
(15) Colton, J. S.; Suh, N. P. *Polym. Eng. Sci.* **1987**, *27*, 485−492.
(16) Colton, J. S.; Suh, N. P. *Polym. Eng. Sci.* **1987**, *27*, 493−499.
(17) Kumar, V.; Suh, N. P. *Polym. Eng. Sci.* **1990**, *30*, 1323−1329.
(18) Kumar, V.; Weller, J. E. *Int. Polym. Process.* **1993**, *8*, 73−80.
(19) Baldwin, D. F.; Park, C. B.; Suh, N. P. *Polym. Eng. Sci.* **1996**, *36*, 1437−1445.
(20) Baldwin, D. F.; Park, C. B.; Suh, N. P. *Polym. Eng. Sci.* **1996**, *36*, 1446−1453.
(21) Kumar, V. *Cell. Polym.* **1996**, *12*, 207−222.
(22) Arora, K. A.; Lesser, A. J.; McCarthy, T. J. *Macromolecules* **1998**, *31*, 4614−4620.
(23) Krause, B.; Sijbesma, H. J. P.; Münüklü, P.; van der Vegt, N. F. A.; Wessling, M. *Macromolecules* **2001**, *34*, 8792−8801.
(24) Krause, B.; Diekmann, K.; van der Vegt, N. F. A.; Wessling, M. *Macromolecules* **2002**, *35*, 1738−1745.
(25) Yokoyama, H.; Sugiyama, K. *Macromolecules* **2005**, *38*, 10516−10522.
(26) Hergenrother, P. M. *Macromolecules* **1981**, *14*, 898−904.
(27) Hofer, D. C.; Allen, R.; Wallraff, G.; Ito, H.; Breyta, G.; Brock, P.; DiPietro, R.; Conley, W. *J. Photopolym. Sci. Technol.* **1996**, *9*, 387−398.
(28) MacDonald, S. A.; Willson, C. G.; Fréchet, J. M. J. *Acc. Chem. Res.* **1994**, *27*, 151−158.
(29) Ichikawa, R.; Hata, M.; Okimoto, N.; Oikawa-Handa, S.; Tsuda, M. *J. Polym. Sci., Part A: Polym. Chem.* **1998**, *36*, 1035−1042.
(30) Ahn, K. D.; Lee, Y. H.; Koo, D. *Polymer* **1992**, *33*, 4851−4856.
(31) Notario, R.; Quijano, J.; Sanchez, C.; Vélez, E. *J. Phys. Org. Chem.* **2005**, *18*, 134−141.
(32) Greene, T. W.; Wuts, G. M. In *Protective Groups in Organic Synthesis*, 2nd ed.; Wiley: New York, 1991; p 327.
(33) Bodensky, M. In *Principles of Peptide Chemistry*; Springer: New York, 1984; p 99.
(34) Flynn, D. L.; Zelle, R. E.; Grieco, P. A. *J. Org. Chem.* **1983**, *48*, 2424−2426.
(35) Hergenrother, P. M. *Macromolecules* **1974**, *7*, 575−582.
(36) Klein, D. J.; Modarelli, D. A.; Harris, F. W. *Macromolecules* **2001**, *34*, 2427−2437.
(37) Guibé-Jampel, E.; Wakselman, M. *Synthesis* **1977**, *11*, 772−773.
(38) Wallraff, G. M.; Hedrick, J. L.; Labadie, J. W. *PMSE Prepr.* **1992**, 289−290.
(39) Unpublished results.
(40) Gain, O.; Seytre, G.; Garapon, J.; Vallet, J.; Sillion, B. In *High-Temperature Properties and Applications of Polymeric Materials*; Tant, M. R., Connell, J. W., McManus, H. L. N., Eds.; ACS Symposium Series; American Chemical Society:Washington, DC, 1995; Vol. 603, pp 22−36.
(41) Khawam, A.; Flanagan, D. R. *Thermochim. Acta* **2005**, *436*, 101−112.
(42) Wallraff, G. M.; Hinsberg, W. D.; Houle, F.; Opitz, J.; Hopper, D. *SPIE* **1995**, *2438*, 182−185.
(43) Tanimura, S.; Kumada, T.; Ueyama, A.; Kobayashi, J.; Kuramoto, K. *Appl. Spectrosc.* **1997**, *51*, 1352−1354.
(44) Hansen, M. M.; Riggs, J. R. *Tetrahedron Lett.* **1998**, *39*, 2705−2706.
(45) Cooper, A. I. *J. Mater. Chem.* **2000**, *10*, 207−234.
(46) Handa, Y. P.; Zhang, Z. *J. Polym. Sci., Part B: Polym. Phys.* **2000**, *38*, 716−725.
(47) Sun, H.; Mark, J. E. *J. Appl. Polym. Sci.* **2002**, *86*, 1692−1701.
(48) Krause, B.; Mettinkhof, R.; van der Vegt, N. F. A.; Wessling, M. *Macromolecules* **2001**, *34*, 874−884.
(49) Siripurapu, S.; DeSimone, J. M.; Khan, S. A.; Spontak, R. J. *Macromolecules* **2005**, *38*, 2271−2280.
(50) Voorhees, P. W. *Annu. Rev. Mater. Sci.* **1992**, *22*, 197−215.
(51) Kumar, V.; Weller, J. E. *Polym. Eng. Sci.* **1994**, *34*, 169−173.
(52) Doshi, P.; Simon, S. *Polym. Eng. Sci.* **2005**, *45*, 640−651.

MA062259T